zol & fai: large-scale targeted detection and evolutionary investigation of gene clusters

Rauf Salamzade[1,2], Patricia Tran[3,4], Cody Martin[2,3], Abigail L. Manson[5], Michael S. Gilmore[5,6,7], Ashlee M. Earl[5], Karthik Anantharaman[3], Lindsay R. Kalan[1,8,9]

[1]Department of Medical Microbiology and Immunology, School of Medicine and Public Health, University of Wisconsin-Madison, Madison, WI, USA
[2]Microbiology Doctoral Training Program, University of Wisconsin-Madison, Madison, WI, USA
[3]Department of Bacteriology, University of Wisconsin-Madison, Madison, WI, USA
[4]Freshwater and Marine Science Doctoral Program, University of Wisconsin-Madison, WI, USA
[5]Infectious Disease and Microbiome Program, Broad Institute of MIT and Harvard, Cambridge, Massachusetts, USA
[6]Department of Ophthalmology, Harvard Medical School and Mass Eye and Ear, Boston, Massachusetts, USA
[7]Department of Microbiology, Harvard Medical School and Mass Eye and Ear, Boston, Massachusetts, USA
[8]Department of Medicine, Division of Infectious Disease, School of Medicine and Public Health, University of Wisconsin-Madison, Madison, WI, USA
[9]M.G. DeGroote Institute for Infectious Disease Research, David Braley Centre for Antibiotic Discovery, Department of Biochemistry and Biomedical Sciences, McMaster University, Hamilton, Ontario, Canada

Address for Correspondence: Lindsay R. Kalan; kalanlr@mcmaster.ca

Abstract

Many universally and conditionally important genes are genomically aggregated within clusters. Here, we introduce fai and zol, which together enable large-scale comparative analysis of different types of gene clusters and mobile-genetic elements (MGEs), such as biosynthetic gene clusters (BGCs) or viruses. Fundamentally, they overcome a current bottleneck to reliably perform comprehensive orthology inference at large scale across broad taxonomic contexts and thousands of genomes. First, fai allows the identification of orthologous or homologous instances of a query gene cluster of interest amongst a database of target genomes. Subsequently, zol enables reliable, context-specific inference of protein-encoding ortholog groups for individual genes across gene cluster instances. In addition, zol performs functional annotation and computes a variety of statistics for each inferred ortholog group. These programs are showcased through application to: (i) longitudinal tracking of a virus in metagenomes, (ii) discovering novel population-genetic insights of two common BGCs in a fungal species, and (iii) uncovering large-scale evolutionary trends of a virulence-associated gene cluster across thousands of genomes from a diverse bacterial genus.

Introduction

Within bacterial genomes, genes are often co-located within smaller genetic structures such as operons[1,2], phages[3], metabolic gene clusters[4], biosynthetic gene clusters (BGCs)[5], and pathogenicity islands [6,7]. Although less prevalent, eukaryotic genomes also contain genes aggregated within discrete clusters[5,8].

Sometimes gene clusters are highly conserved, encoding for products essential to the survival of the organism[9]. In other cases, a single gene cluster can exhibit variability in gene carriage and order across different strains or species[10–12]. This is often the case for BGCs

encoding specialized metabolites or virulence-associated gene clusters, where evolution of gene content and sequence divergence can influence fitness and contribute to adaptation within a changing ecosystem.

Bioinformatic toolkits to perform accurate pangenomic and comparative genomic analyses have been heavily developed over the past two decades[13–18]; however, tool development to aid the identification and comparative analysis of smaller homologous gene clusters has been more limited and largely designed for specific types of gene clusters[19–22]. In addition, while methods for comprehensive comparative genomics within species exist and are scalable[17,23,24], methods for reliable, large-scale comparative genomics of thousands of genomes representing a greater breadth of taxonomic diversity are lacking and bear heavy computational costs[25,26]. Context-specific inference of orthologous genes within focal gene clusters offers a targeted and reliable solution to overcome challenges with scalability[27,28]. Such an approach was recently taken to infer orthologous genes between instances of homologous BGCs[22].

Here, we introduce fai (*find-additional-instances*) and zol (*zoom-on-locus*), which are designed for the identification (fai) and in-depth evolutionary genomics investigations (zol) of a wide array of gene cluster types. We demonstrate the utility of these programs through application to three types of gene clusters within different genomic contexts including a novel bacteriophage within environmental metagenomes, a fungal secondary metabolite encoding biosynthetic gene clusters, and a conserved polysaccharide antigen locus within the diverse bacterial genus of *Enterococcus*.

Results

fai and zol allow for the rapid inference of gene cluster orthologs across diverse genomes

The two programs, fai and zol, build upon approaches we recently reported in *lsa*BGC[29] that were developed to investigate evolutionary trends of BGCs in a single taxon. Within fai and zol, algorithmic adjustments have been implemented to broaden the application for searching any type of gene cluster across a diverse set of target genomes (Figure 1A). First, fai allows users to rapidly search for gene cluster instances in a target set of genomes. Then, zol can be used to compute evolutionary statistics and functional annotations of gene cluster content in table-based reports. Importantly, because fai has an option to filter secondary, potentially paralogous, instances of gene clusters found in target genomes, downstream *ab initio* clustering of proteins using a flexible, InParanoid-type algorithm[14] by zol can be used to reliably infer ortholog groups.

In addition to filtering secondary instances of query gene clusters identified in target genomes, detection criteria in fai can be adjusted by assessing whether gene cluster homologs lie near scaffold edges in target genomic assemblies. This feature overcomes challenges inherent to the identification of full gene-clusters in metagenomic assemblies or metagenome-assembled genomes, which can be highly fragmented (Figure S1). fai can further accept query gene-clusters in different formats to ease searching for gene clusters and genomic islands cataloged in databases such as ICEberg[30], MIBiG[31], or IslandViewer[32]. In addition, to promote

consistency in gene calling across target genomes, we have incorporated computationally light-weight dependencies for *de novo* gene prediction in prokaryotic genomes[33,34] and gene-mapping in eukaryotic genomes[35] within prepTG, to prepare and format target genomes for optimized gene-cluster searching in fai (Figure 1B). Together these unique features and options differentiate fai from other software with similar functionalities, such as cblaster[21] (Figure 1C, S1; Table S1; Supplementary Text).

zol is differentiated from *lsa*BGC[29], where ortholog groups are inferred across full genomes using OrthoFinder[18], by delineating ortholog groups within the context of a homologous or orthologous set of gene clusters, similar to the approach taken within CORASON[22] to visualize similarities between BGCs. While CORASON uses bidirectional best-hits to identify direct orthologs, zol accounts for the presence of in-paralogs and comprehensively partitions proteins into ortholog groups. Similar to *lsa*BGC-PopGene[29], zol will then construct a tabular report with information on conservation, evolutionary trends, and annotation for individual ortholog groups (Figure 1D). To make annotated reports generated by zol more broadly informative for a variety of gene clusters, several databases have been included, such as VOGs[36], VFDB[37], ISFinder[38], and CARD[39]. In addition, zol incorporates HyPhy[40] as a dependency and calculates evolutionary statistics not previously reported in *lsa*BGC-PopGene, such as sequence entropy in the 100 bp upstream of an ortholog group, where important regulatory differences could exist[41]. Ultimately, beyond high-throughput inference of ortholog groups across diverse genomic datasets, the rich tabular report produced by zol provides complementary information to figures generated by comparative visualization software such as clinker[42], CORASON[22], gggenomes[43], and Easyfig[44].

Another key feature in zol is the ability to dereplicate gene clusters directly using skani[45], which was recently shown to be more reliable at estimating ANI between genomes of variable contiguity relative to comparative methods. Dereplication allows for more appropriate inference of evolutionary statistics to overcome availability or sampling biases in genomic databases[46]. Finally, zol allows for comparative investigations of gene-clusters based on taxonomic or ecological groupings[47–49]. For instance, users can designate a subset of gene clusters as belonging to a specific population to allow zol to calculate ortholog group conservation across just the focal set of gene clusters. In addition, if comparative investigations are requested, zol will also compute the fixation index[50], F_{ST}, for each ortholog group to assess gene flow between the focal and complementary sets of gene clusters.

Longitudinal tracking of a virus within lake metagenomic assemblies

Viruses are important members of host and environmental microbiomes[51–53], influencing the microbial composition and participating in several metabolic pathways. Targeted identification of a specific virus or bacteriophage within metagenomes can thus offer greater insight into their elusive functional roles in microbiomes.

Recently, changes in the composition and function of the metagenome at three different depths of a lake was reported using longitudinal shotgun metagenomics[54]. Using metagenome assemblies generated from this dataset, large (≥20kb) and predicted-circular phages were identified independently across a subset of metagenomes from the three different depths at the the earliest sampling date using VIBRANT[55]. Subsequent clustering based on the sequence and

syntenic similarity of protein domains identified a ~36kb highly conserved virus in two metagenomes sampled from lower lake depths.

fai was then used to perform a rapid, targeted search for this ~36kb *Caudovirales* virus across the full set of 16 metagenomes to identify additional instances of the virus. fai completed its search of the metagenomes, featuring >20 million proteins and 10.7 million contigs, in less than seven minutes using 20 threads. Of the 16 total metagenomes, spanning five distinct sampling timepoints and four distinct sampling depths, nine metagenomes containing the virus were identified (Figure 2A) exclusively from anoxic conditions (p=8.7e-5; two-sided Fisher's exact test). This suggests the viral host likely performs anaerobic respiration. Application of zol further revealed that 34 (64%) of the 53 total distinct ortholog groups were core to all instances of the virus across nine metagenomes and completely conserved in sequence over the course of 2.5 months (Figure 2B; Table S2). Furthermore, seven of the 53 ortholog groups were not observed in the query viruses from the earliest sampling date, demonstrating the ability of fai to identify new genes within additional instances of known gene clusters.

Investigating population-level and species-wide evolutionary trends of BGCs in the eukaryotic species *Aspergillus flavus*

The fungal genus of *Aspergillus* is a source of several natural products, including aflatoxins, a common and economically impactful contaminant of food. The genus also contains species that are model organisms for studying fungal secondary metabolism[56–58]. Examination of the secondary metabolome of *A. flavus* has revealed that different clades or populations comprising certain species can exhibit variability in their metabolite production despite high conservation of core BGC genes encoding enzymes for synthesis of these metabolites[12,59,60]. For instance, population B *A. flavus* were identified as producing a greater abundance of the insecticide leporin B relative to populations A and C[12,61].

To further understand the genomic basis for differences in metabolite content between populations, we investigated the leporin BGC using fai and zol. While the leporin cluster was previously identified as a core component of the *A. flavus* genome[12], a recent study suggested that the full BGC was specific to a single clade from the species[60]. Low sensitivity in direct assessment of gene cluster presence in eukaryotic genome assemblies can arise from their incompleteness, leading to gene clusters being fragmented across multiple scaffolds, and challenges in *ab initio* gene prediction[62,63]. Further deterring the direct prediction of gene clusters in eukaryotic assemblies is the lack of gene annotations, with only 11 (5.1%) of 216 *A. flavus* genomes in NCBI's GenBank database having coding sequence predictions (Figure 3A). Therefore, we used miniprot[35], which is integrated within prepTG, to directly map high-quality coding genes predictions based on transcriptomics data from the genome of strain *A. flavus* NRRL 3357[64] to the 216 genomes available for the species. Running fai in "draft mode" led to the identification of the leporin BGC within 212 (98.1%) assemblies, consistent with prior read mapping-based investigations[12]. This increase in sensitivity when fai is run with miniprot-based gene-mapping is substantial when compared to common alternate approaches for identifying homologous instances of BGCs across genomes (Figure 3B; Supplementary Text).

Of the 212 genomes with the leporin BGC, 202 contain instances that were not near scaffold edges. This set of 202 instances of the gene cluster were further investigated using zol,

with comparative investigation of BGC instances from *A. flavus* population B genomes to instances from other populations requested. High sequence conservation was observed for all genes in the leporin gene cluster as previously reported[12] (Table S3). Further, alleles for genes in the BGC from population B genomes were generally more similar to each other than to alleles from outside the population as indicated by high F_{ST} values (>0.85 for 9 of 10 genes) (Figure 3C; Table S3). While regulation of secondary metabolites in *Aspergillus* is complex[65], zol analysis showed that the three essential genes for leporin production[61] also had the lowest variation in the 100 bps upstream their exonic coordinates (Figure S2). This suggests higher variability is occurring in the transcription of the accessory *lep* genes within the species. This supports experimental evidence that has shown gene knockouts depleting certain leporin species will still permit the production of others[61].

fai and zol were also applied to the BGC encoding aflatoxin across *A. flavus*[66] (Table S4). Similar to the leporin BGC, the aflatoxin BGC was highly prevalent in the species and found in 71.8% of genomes. However, in contrast to the leporin BGC, the aflatoxin BGC contains several genes with positive Tajima's D values, indicating greater sequence variability for these coding regions across the species (Figure 3D). One of the genes with a positive Tajima's D value is *aflX*, which has been shown to influence conversion of the precursor veriscolorin A to downstream intermediates in the aflatoxin biosynthesis pathway[67] (Figure 3E). An abundance of sites with mid-frequency alleles in the oxidoreductase encoding gene could represent granular control for the amount of aflatoxin relative to intermediates produced. The polyketide synthase gene *pksA* had the lowest Tajima's D value of -2.4, which suggests it is either highly conserved or under purifying selection (Figure 3F). In addition, because a recent predicted reference proteome was used to infer genomic coding regions, fai and zol detected several highly conserved genes within the aflatoxin BGC that are not represented in the original reference gene cluster input for fai[31]. This includes a gene annotated as a noranthrone monooxygenase recently characterized as contributing to aflatoxin biosynthesis[68,69] (Figure 3D).

Large-scale identification of the Enterococcal polysaccharide antigen and assessment of context restricted orthology inference

The Enterococcal polysaccharide antigen (Epa) is a signature component of the cellular envelope of multiple species within *Enterococcus*[70–73], which has mostly been characterized in the species *Enterococcus faecalis*[70,74–77]. While molecular studies have provided evidence that the locus contributes to enterococcal host colonization[76], evasion of immune systems[78], and sensitivity to antibiotics[79] and phages[79,80], it was only recently that the structure of Epa was resolved and a model for its biosynthesis and localization formally proposed[77]. A homologous instance of the *epa* locus was identified in the other prominent pathogenic species from the genus, *Enterococcus faecium*[71,73,81]; however, the prevalence and conservation of *epa* across the diverse genus of *Enterococcus*[82–84] remains poorly studied.

fai was used to search for homologous instances of *epa* across 5,291 *Enterococcus,* genomes estimated by GTDB to represent 92 species[85], using a sensitive searching criterium and coordinates of the locus along the *E. faecalis* V583 genome as a reference[75,77] (Supplementary Text). For detection of *epa* orthologous regions, co-location of at least seven of the 14 *epa* genes previously identified as conserved in both *E. faecalis* and *E. faecium* was

required. The default threshold for syntenic conservation of homologous instances to the query gene cluster was also disregarded to increase sensitivity for the detection of *epa* in more distantly related enterococcal species to *E. faecalis*. To allow for capture and downstream analysis of auxiliary genes which might be species or strain-specific but related to Epa production or decoration, 20 kb flanking contexts of the core *epa* genes identified in each target genome were extracted.

Using these criteria, 5,085 (96.1%) genomes from across the genus were found to possess an *epa* locus, confirming the locus as nearly core to the genus. Visual inspection of the *epa* genes among 463 representative *Enterococcus* genomes revealed that the core genes *epa*A-*epa*R are highly conserved in three of four major clades (Figure 4; Supplementary Text). Based on the detection criteria in fai, the *epa* locus in the fourth clade, previously referred to as the *Enterococcus columbae* group[82], was either missing or encoded for highly divergent homologs of these genes. This clade includes *Enterococcus gallinarum*, one of the only other species in the genus, besides *E. faecalis* and *E. faecium,* reported to cause nosocomial outbreaks[86,87].

Evolutionary trends and sequence diversity for individual genes with the *epa* locus, were next computed using zol after assessing zol's reliability for gene cluster context-limited inference of orthology and the impact of dereplication on the calculation of evolutionary statistics by zol.

Gene-context specific orthology inference using fai and zol are concordant with genome-wide ortholog group predictions

Genome-wide orthology inference is currently difficult to scale to hundreds or thousands of genomes belonging to multiple species. However, orthology inference can be made more accessible if larger loci are first identified as orthologous between genomes, through leveraging syntenic support[23,27]. To assess whether ortholog group inference was reliable when zol is applied on orthologous gene clusters identified across multiple species, we ran zol on high-quality instances of the *epa* locus from 42 different species (Figure 5C). Ortholog group predictions by zol were then compared to genome-wide orthology predictions by OrthoFinder[18], which has been shown to yield highly accurate predictions in benchmarking experiments involving genomes from multiple species[88]. Orthology predictions were highly concordant between zol and OrthoFinder for proteins from diverse instances of the *epa* locus. zol identified 23,623 pairs of proteins within ortholog groups, of which 22,843 (96.70%) were also grouped together by OrthoFinder. Only 1,520 (6.24%) pairs of *epa*-associated proteins which were identified by OrthoFinder to belong to the same ortholog group were missed by zol.

Because the *epa* locus encodes multiple characterized and putative glycosyltransferases[89], we used phylogenetics to examine the relationship between proteins belonging to ortholog groups with glycosyltransferase domains to confirm that major clades correspond to distinct ortholog group designations (Figure 5B). zol also has an option to "re-inflate" ortholog groups, expanding them to include proteins from gene clusters which were deemed redundant during dereplication. To demonstrate the scalability of zol, this "re-inflation"-based approach was next applied on the full set of high-quality and contiguous *epa* instances and a comprehensive phylogeny of ortholog groups corresponding to glycosyltransferases was constructed. In concordance with our analysis of the 42 representative genomes, distinct

phylogenetic clades for glycosyltransferases corresponded to different ortholog groups identified by zol (Figure 5C).

Dereplication can impact taxa-wide inferences of selection-informative statistics

Dereplication, or removal of redundant gene cluster instances, is important to consider when working with highly sequenced bacterial taxa, including *E. faecalis*, where certain lineages, such as those commonly isolated at clinics, can be overrepresented in genomic databases. Over-representation of select lineages will skew estimates for some evolutionary statistics, such as those informative of selective pressures, complicating evaluation of evolutionary trends across the entire taxonomic group. We thus assessed the impact of dereplication on the calculation of evolutionary statistics for instances of *epa* in *E. faecalis* using two different approaches: (i) genome-wide dereplication with dRep[90,91] and (ii) gene cluster specific dereplication with skani[45]. Dereplication at the gene cluster level with skani was performed directly in zol. The “re-inflation” option was also used to simulate comprehensive processing and calculation of evolutionary statistics while avoiding excessive computation.

Regardless of the approach for dereplication, genome-wide or gene cluster-specific, the estimates of evolutionary and genomic statistics for analogous ortholog groups were highly concordant (Figure 6, S3). However, gene cluster based dereplication can overestimate or underestimate selection informative statistics, such as Tajima’s D or FUBAR-based inference of the number of sites under selection, relative to genome-wide dereplication performed using similar thresholds. This is likely because the core *epa* locus is highly conserved across *E. faecalis* which led to fewer representative gene clusters following dereplication and a lower weight being placed on conserved alleles when estimating such statistics. In contrast, more simplistic statistics, such as average sequence entropy and the proportion of total alignment sites regarded as segregating sites, were closely estimated for genes regardless of the dereplication method used. In addition, using the “reinflation” option in zol to infer orthology relationships across a comprehensive set of 1,232 high-quality and contiguous *epa* locus instances from the species produced concordant values for selection informative statistics to values generated using genome-wide based dereplication.

zol identifies genetic diversity of *epa*X-like glycosyltransferases

Because Epa biosynthesis and its conditional importance has mostly been investigated in *E. faecalis*[70,74,75,77], we first examined evolutionary trends for proteins across instances of the *epa* locus from 75 *E. faecalis* representative genomes following genome-wide dereplication. In accordance with prior studies[71,77], zol reported that one end of the locus corresponds to genes which are highly conserved and core to *E. faecalis* (*epa*A-*epa*R) whereas the other end contains strain-specific genes (Figure 7A; Table S5). Using zol, we further found that variably conserved genes exhibit high sequence dissimilarity, as measured using both Tajima’s D and average sequence entropy, in comparison to the core genes of the locus (Figure 7BC). Comparative and multi-species analysis of the *epa* locus between and across *E. faecalis* and *E. faecium* was next performed using gene cluster based dereplication with re-inflation using zol (Table S6). zol reported conservation statistics were consistently in agreement with previous studies[71,73].

Twenty genes determined to be present in the majority (>95%) of *epa* clusters across both species, including *epa*ABCDEFGH, *epa*LM, and *epa*OPQR. In addition, default parameters for orthologous clustering of proteins in zol detected a known truncated variant of the glycosyltransferase *epa*N in *E. faecium*.

The gene *epaX,* encoding a glycosyltransferase, was identified as one ortholog group with the greatest sequence variation in *E. faecalis* (Figure 7BD, S4). *epa*X was previously shown to be critical for *E. faecalis* host-gut colonization and proposed to be involved in the decoration of the rhamnan backbone structure of Epa with galactose and N-acetyl glucosamine[76]. Comparative analysis using *E. faecium* as the focal taxa further showed that the *epa*X-containing ortholog group has a low F_{ST} value, indicating alleles from *E. faecalis* and *E. faecium* species are phylogenetically interspersed. This was confirmed through phylogenetic assessment of the ortholog group (Figure 7E). In addition, although some allelic clades encode sequences from both species, genes remained sub-partitioned by species. This phylogenetic structure for the ortholog group, together with our prior observation that the *epa*X-containing ortholog group in *E. faecalis* has greater sequence variability relative to other glycosyltransferases from the locus, suggests extensive and ancestral sequence evolution of *epa*X-like glycosyltransferases. Further, while only 70% of *E. faecium* found to carry *epa* possess an *epa*X-like ortholog group, approximately 7% of them encode the ortholog in multi-copy (Figure 7F), suggesting the occurrence of intra-locus gene duplication.

Discussion

Here fai and zol are introduced to enable large scale evolutionary investigations of gene clusters in diverse taxa. Together these tools overcome current bottlenecks in computational biology to infer orthologous sets of genes at scale across thousands of diverse genomes.

Both fai and cblaster[21] can be used to identify additional gene clusters within target genomes and extract them as GenBanks for downstream investigations using zol. For those lacking computational resources needed for fai analysis, cblaster offers remote searching of BGCs using NCBI's BLAST infrastructure and non-redundant databases. More recently, CAGECAT[92], a highly accessible web-application for running cblaster, was also developed and can similarly be used to identify and extract gene cluster instances from genomes represented in NCBI databases. In contrast to these tools, fai contains algorithms and options for users interested in: (i) identifying gene clusters across a comprehensive or redundant set of genomic assemblies, (ii) improved sensitivity for gene cluster detection in draft-quality assemblies, and (iii) automated filtering of secondary, or paralogous, matches to query gene clusters. In addition, users can apply zol to further investigate homologous sets of gene clusters identified from IslandCompare[93], BiG-SCAPE[22], or vConTACT2[94] analyses, which perform comprehensive clustering of predicted genomic islands, BGCs, or viruses.

The utility of fai is demonstrated here through rapid, targeted detection of a virus directly from lake metagenomic assemblies. Targeted detection of specific viruses longitudinally presents an efficient and tractable approach to understand how viral pangenomes evolve over time. In addition, by permitting fragmented detection of gene clusters and detection of proximity to scaffold edges, users can assess whether phages or other gene clusters corresponding to MGEs are present in their metagenomes. fai and zol will continue to compliment metagenomic

applications as long-read sequencing becomes more economical and commonly used to profile microbial communities. For example, their application could be useful for assessing the presence of concerning MGEs conferring antimicrobial resistance traits[95–97] and identifying novel auxiliary genes within known BGCs which may tailor the resulting specialized metabolites and expand chemical diversity[98,99].

Reidentifying gene-clusters in eukaryotic genomes remains difficult due to technical challenges in gene prediction owing to the presence of alternative splicing. The ability of fai and zol to perform population-level genetics on common BGCs from the eukaryotic species *A. flavus* was demonstrated. While there are over 200 genomes of *A. flavus* on NCBI, only 5.1% have coding-sequence information readily available. We used miniprot[35] to map high quality gene coordinate predictions from a representative genome in the species[64] to the remainder of genomic assemblies within prepTG which enabled high sensitivity detection of BGCs with fai. Our analysis provides additional support that the leporin BGC is conserved in full across the species[12] using an assembly-based approach.

Application of fai and zol to exopolysaccharide encoding gene clusters from pathogens of interest allows a better understanding of their conservation and evolutionary trends. This information can then aid the identification of potential genes to target for antivirulence efforts[103,104] or genes underlying host-pathogen interactions[76,105]. fai was used to identify orthologous instances of the *epa* locus, encoding for an extracellular polysaccharide antigen, across thousands of diverse genomes from the genus of *Enterococcus*. Subsequently, application of zol reliably produced comparable orthology predictions to OrthoFinder, a highly dependable genome-wide orthology inference software[18,88]. While zol missed a small percentage of orthologous instances identified by OrthoFinder in our testing, this could be due to threshold settings for percent identity and coverage between pairs of proteins set in zol. Such thresholds are not enforced in OrthoFinder. However, parameters controlling these thresholds are adjustable in zol and allow users to increase or decrease orthology sensitivity at the expense of incurring false positives as they deem appropriate for their research objective.

Using zol, it was determined that an ortholog group containing *epa*X-like glycosyltransferases possess high sequence divergence relative to other glycosyltransferases within the *epa* locus in *E. faecalis*. In addition to influencing the ability of *E. faecalis* to colonize hosts[76], mutations in *epa*X and other genes from the ortholog group have also been shown to impact susceptibility to phage predation[100–102]. Thus, because similar *epa*X-like glycosyltransferases are found in both *E. faecalis* and *E. faecium*, we hypothesize that extensive ancestral evolution of the *epa*X-containing ortholog group may have occurred to support evasion from phages and confer colonization of new hosts. In this study, we further found that the *E. columbae* group might lack or possess highly divergent versions of core *epa* genes found in *E. faecalis* and *E. faecium*, suggesting that development of anti-virulence approaches to broadly target Epa in all pathogenic enterococci might be difficult to achieve. Similar investigations with fai and zol can readily be performed for other exopolysaccharide encoding gene clusters of pathogens to better understand their conservation, evolutionary trends, identify appropriate genes to target for antivirulence efforts[103,104], and infer whether certain genes underlie host-pathogen interactions[76,105].

Options for dereplication and re-inflation provided within zol enable scalability to thousands of gene cluster instances. The usage of these options can further aid in performing

more accurate evolutionary investigations for genes broadly across focal taxa or between clades, by overcoming biases due to overrepresentation of certain lineages in genomic databases[12,47]. Depending on the underlying origin of input gene clusters, zol can also be used to assess temporal[48,106] or spatial[49] evolutionary trends.

Practically, zol presents a comprehensive analysis tool for comparative genetics of related gene clusters to facilitate detection of evolutionary patterns that might be less apparent from visual analysis. Fundamentally, the algorithms presented within fai and zol enable the reliable detection of orthologous gene clusters, and subsequently orthologous proteins, across multi-species datasets spanning thousands of genomes and help overcome a key barrier in scalability for comparative genomics.

Acknowledgments

This work was supported by grants from the National Institutes of Health awarded to L.R.K (NIAID U19AI142720 and NIGMS R35GM137828) and the Broad Institute (U19AI110818). The content is solely the responsibility of the authors and does not necessarily represent the official views of the National Institutes of Health. The authors are grateful to James Kosmopoulos, Dr. Caitlin Sande, and Mary Hannah Swaney for feedback and assistance with data acquisition as well as Dr. Devon Ryan and Dr. Robert A. Petit III for assistance with incorporation of the suite into Bioconda.

Methods

Software availability

zol is provided as an open-source software suite, developed primarily in Python3 on GitHub at: https://github.com/Kalan-Lab/zol. Docker and Bioconda[107] based installations of the suite are supported. For the analyses presented in this paper, we used v1.2.0 of the zol software package. Minor patches, since incorporated into the software since v1.25, were added retrospectively to this version pertaining to safer acquisition of stored statistics when generating the final report. Version information for major dependencies of the zol suite[33,35,40,45,108–115] or software generally used[22,55,116] for analyses in this study is provided in Supplementary Table S7.

Data availability

Genomes and metagenomes used to showcase the application of fai and zol are listed with GenBank accession identifiers in Supplementary Table S8. Total metagenomes and their associated information from Lake Mendota microbiome samplings were originally described in Tran *et al.* 2023[54] and deposited in NCBI under BioProject PRJNA758276. Genomic assemblies available for *A. flavus* in NCBI's GenBank database on Jan 31st, 2023 were downloaded in GenBank format using ncbi-genome-download (https://github.com/kblin/ncbi-genome-download). Genomic assemblies for *Enterococcus* that met quality and taxonomic criteria for belonging to the genus or related genera (e.g. Enterococcus_A, Enterococcus_B, etc.) in GTDB[85] release R207 were similarly downloaded from NCBI's GenBank database using ncbi-genome-download in FASTA format.

Application of fai and zol to identify phages within metagenomes

VIBRANT was used to identify viral contigs or sub-contigs in the three total metagenomes from Tran *et al.* 2023[54] sampled on the earliest date of 07/24. Afterwards, predicted circular contigs were clustered using BiG-SCAPE[22] which revealed a ~36 kb virus was found in two of the three metagenomes.

prepTG was run on all 16 total metagenomic assemblies from the Tran *et al.* 2023 study, performing gene calling with pyrodigal in metagenomics mode[33] to prepare for comprehensive targeted searching of the virus. Afterwards, fai was run with default settings, with filtering of paralogous (or secondary) instances of the phage requested to retain only the best matching scaffold or scaffold segment resembling the queries.

Microevolutionary investigations of leporin and aflatoxin BGCs in *Aspergillus flavus*

Genomic assemblies downloaded from NCBI GenBank were processed using prepTG. Of the 217 genomic assemblies downloaded, one, GCA_000006275.3, was dropped from the analysis because the original GenBank had multiple CDS features with the same name, leading to difficulties in performing BGC prediction with antiSMASH[116], and because alternate assemblies were available for the isolate. prepTG was run on all assemblies with miniprot[35] based gene-mapping of the high-quality gene coordinate predictions available for *A. flavus* NRRL 3357 (GCA_009017415.1)[64] requested. Target genomes were then searched for the leporin (BGC0001445) and aflatoxin (BGC0000008) BGCs using GenBanks provided on MIBiGv3[31]. For leporin, AFLA_066840, as represented in the MIBiG database, was treated as a key protein required for detection of the BGC. Similarly, for aflatoxin, PksA (AAS90022.1), as represented in the MIBiG database, was treated as a key protein required for detection of the BGC. Draft-mode and filtering of paralogous segments was requested but turned off by default.

We reidentified population B as previously delineated[12] using k-mer based ANI estimation[117] and neighbor-joining tree construction[118]. A discrete clade (n=81) in the tree was validated to feature all isolates previously determined as part of population B[12] and thus regarded as such.

For comprehensive and *de novo* BGC prediction, antiSMASH was run on the 216 genomic assemblies with ‘glimmerhmm’ requested for the option ‘--genefinding-tool’. BGCs were clustered using default settings in BiG-SCAPE with MIBiG reference BGC integration requested and a PKS-NRPS hybrid GCF was found to feature the leporin B BGC representative (BGC0001445). Only 65 (30.1%) of the 216 genomic assemblies featured this GCF, likely resulting from the use of distant gene models based on *Cryptococcus* genomes with glimmerhmm[119]. For remote clinker analysis, CAGECAT[92] was used to search NCBI’s nr database with proteins from the leporin BGC representative (BGC0001445) provided as a query. Only 13 scaffolds, belonging to 12 assemblies (including GCA_000006275.3), were identified.

Evolutionary investigations of the *epa* locus across *Enterococcus*

All *Enterococcus* genomes represented in GTDB R207[85] (n=5,291) were downloaded using ncbi-genome-download and processed in prepTG with gene-calling performed using pyrodigal[33]. Coordinates extending from 2,071,671 to 2,115,174 along the *E. faecalis* V583 chromosome, corresponding to genes EF2164 to EF2200. When using direct coordinates along a reference, fai reperforms gene-calling along the reference and extracts a local GenBank corresponding to the region between the coordinates. Gene calling is performed using pyrodigal. Because prior comparative analyses had shown that gene-conservation and gene-order can be slightly variable between epa loci from *E. faecalis* and *E. faecium*[71], we relaxed the syntenic similar to query in fai from 0.6 to 0.0 and minimum percentage of query proteins needed to report a homologous instance of the *epa* locus to 10%. Instead, we required the presence of 50% of key *epa* proteins found in both *E. faecalis* and *E. faecium*, *epaABCDEFGHLMOPQR*, for the identification of valid homologous instances of the *epa* locus. To gather auxiliary genes flanking the core *epa* regions detected, we further requested the inclusion of CDS features found within 20 kb of the boundary core *epa* genes.

Genome selection for comparing ortholog grouping of proteins by zol with OrthoFinder: Genome-wide dereplication of all *Enterococcus* genomes using dRep[90] with fastANI[91] and a secondary ANI clustering threshold of 99.0% led to the identification of 463 distinct genomes, including 101 *E. faecalis* genomes. Of these 101 genomes, 75 had high-quality *epa* instances which were not located near scaffold edges. zol was run on the 75 high-quality *epa* instances using default ortholog grouping parameters and similarly OrthoFinder v2.5.4 was run using default settings on the full, genome-wide set of 75 proteomes. To assess the concordance between OrthoFinder and zol for more diverse gene-clusters, gathered from multiple species, dRep was applied a second time on the set of 463 *Enterococcus* genomes using an ANI threshold of 95.0% to approximate selection of one representative genome per species[120]. This secondary dereplication identified 89 genomes, of which 42 featured highly-quality instances of the *epa* locus.

Phylogenetic analysis of glycosyltransferases found in or near the epa locus: Ortholog groups from the zol analysis on the 42 representative and 2,442 comprehensive multi-species *epa* instances (Figure 5BC), as well as the 75 representative *E. faecalis epa* instances (Figure S4), were identified as glycosyltransferases if they featured the key words: “glycosyl” and “transferase” in Pfam protein domain annotations[121]. For each gene cluster set, protein sequences belonging to the ortholog groups were extracted, retaining association information with particular ortholog groups, and subsequently aligned using MUSCLE[115]. Alignment filtering was next performed using trimal with options “-keepseqs -gt 0.9”, sequences with greater than 25% of sites being gaps were filtered, and an approximate maximum-likelihood phylogeny was finally constructed using FastTree2[110], midpoint rooted, and visualized using iTol[122]. Ortholog groups were assigned to specific *epa* gene designations based on sequence alignment of *E. faecalis* V583 proteins.

Assessing the impact of dereplication on the calculation of evolutionary statistics computed by zol: To assess the impact of dereplication on the estimation of evolutionary statistics using zol, we focused on high-quality instances (<10% of bases ambiguous) of the *epa* locus that were not near scaffold edges from *E. faecalis* genomes. We ran dereplication at the genome scale using dRep[90] with fastANI[91] and a secondary ANI clustering threshold of 99.0% and dereplication at the gene-cluster scale using skani[45] at 99.0% identity and 99.0% coverage with single-linkage clustering. We additionally simulated comprehensive processing of all high-quality gene-clusters distant from scaffold edges using the re-inflation option in zol, which allows expansion of ortholog groups determined in the dereplicated gene cluster set to the full listing of gene-clusters. Comparisons of estimates for various evolutionary statistics by zol between the different dereplication approaches were performed by first identifying the best matching ortholog groups from the three distinct analyses to each *epa*-associated gene from EF2164 to EF2200 in the *E. faeacalis* V583 reference genome based on E-value. Only ortholog groups which were found in single-copy within the *epa* context were considered.

Figure Legends

Figure 1: Overviews of fai and zol. A) A schematic of how prepTG, fai, and zol are integrated to perform evolutionary investigations by searching for gene clusters. An overview of the prepTG (**B**), fai (**C**) and zol (**D**) algorithms and workflows.

Figure 2: Targeted viral detection in metagenomes using fai. A) Total metagenomes from a single site in Lake Mendota across multiple depths and timepoints from Tran et al. 2023 were investigated using fai for the presence of a virus found in two of the three earliest microbiome samplings (red box). The presence of the virus is indicated by a phage icon. Metagenome samples are colored according to whether they corresponded to oxic, oxycline, or anoxic. The most shallow sampling depths varied for different dates and consolidated as a single row corresponding to a sampling depth of either 5 or 10 meters. **B**) The pangenome of the virus is shown based on the consensus order and directionality of coding sequences inferred by zol. Bar heights correspond to the median length of coding sequences and are colored based on the percentages of the nine metagenomes the virus was detected in. Figure 2a was created with BioRender.com.

Figure 3: Evolutionary trends of common BGCs in *A. flavus*. A) The proportion of 216 A. flavus genomes from NCBI's GenBank database with coding-sequence predictions available. **B)** Comparison of the sensitivity of fai and alternate approaches based on assemblies for detecting the leporin BGC. The red-line indicates the total number of genomes (n=216) assessed. A schematic of the (**C**) leporin and (**D**) aflatoxin BGCs is shown with genes present in $\geq$ 10% of samples shown in consensus order and relative directionality. Coloring of genes in (**C**) corresponds to FST values and in (D) to Tajima's D values, as calculated by zol. Grey bars in the legends, at (**C**) 0.92 and (**D**) -0.98, indicate the mean values for the statistics across genes in the BGC. *For the leporin BGC, *lepB* corresponds to an updated open-reading frame (ORF) prediction by Skerker *et al.* 2021 which was the combination of AFLA_066860 and AFLA_066870 ORFs in the MIBiG entry BGC0001445 used as the query for fai. For the aflatoxin BGC, ORFs which were not represented in the MIBiG entry BGC0000008 but predicted to be within the aflatoxin BGC by mapping of gene-calls from *A. flavus* NRRL 3357 by Skerker et al. 2021 are shown in gold. The major allele frequency distributions are shown for (**E**) *aflX* and (**F**) *pksA*, which depict opposite trends in sequence conservation according to their

respective Tajima's D calculations.

Figure 4: The *epa* locus is conserved across most enterococcal species. The distribution of the *epa* locus and associated genes, based on criteria used for running fai, is shown across 463 representative genomes across *Enterococcus*. Coloring of the heatmap corresponds to the normalized bitscore of the best alignment to coding sequences from *E. faecalis* V583.

Figure 5: Assessment of gene-cluster restricted ortholog grouping by fai and zol. A) zol gene-cluster constricted ortholog group predictions for *epa* locus proteins from 42 distinct representative enterococcal species were compared to genome-wide predictions of ortholog groups by OrthoFinder. A phylogeny based on gap-filtered protein alignments of ortholog groups with domains featuring "glycosyl" and "transferase" as key words is shown from (**B**) *epa* loci in the 42 representative genomes and (**C**) a more comprehensive set of 2,442 *epa* loci. Each node represents a specific protein and coloring of the track corresponds to their ortholog group designations by zol. Note, (B) 2 (0.07%) and (C) 79 proteins (0.4%) were removed prior to phylogeny construction due to an abundance of gaps in the trimmed alignment.

Figure 6: Effects of dereplication on the calculation of evolutionary statistics by zol. The heatmap shows the correlation of values for analogous ortholog groups for various evolutionary statistics computed by zol when different approaches to dereplication are used. See Methods for further details. *To simulate no dereplication, gene cluster dereplication with re-inflation parameters were used in zol.

Figure 7: Distribution of the *epa* locus and associated genes across the genus of *Enterococcus*. A) A schematic is shown for the *epa* locus in *E. faecalis* for genes which were found in $\geq$ 25% of 83 representative genomes for the species presented in consensus order with consensus directionality as inferred by zol. The coloring corresponds to the conservation of individual genes. Genes upstream and/or including *epaR* were recently proposed to be involved in decoration of Epa by Guerardel *et al.* 2020. "//" indicates that the ortholog group was not single-copy in the context of the gene cluster. The tracks below the gene showcase their sequence similarity across the *E. faecalis* genomes measured using (**B**) Tajima's D and (**C**) the average sequence alignment entropy. **D**) The major allele frequency is depicted across the alignment for the ortholog group featuring *epaX*. Sites predicted to be under negative selection by FUBAR, Prob(□>□) $\geq$ 0.9, are marked in red. **E**) An approximate maximum-likelihood phylogeny based on gap-filtered codon alignments for the ortholog group corresponding to *epaX* and *epaX*-like proteins in the joint *E. faecalis* and *E. faecium* investigation of the epa locus using zol. **F**) Conservation of *epaX* is shown amongst *E. faecalis* and *E. faecium* genomes with a high-quality representation of the *epa* locus available. Coloring of the bars corresponds to the proportion of genomes with a certain copy-count of the *epaX*-like ortholog group. **G**) The distribution of the epa locus and associated genes, based on high-sensitivity criteria used for running fai, is shown across 463 representative genomes across *Enterococcus*. Coloring of the heatmap corresponds to the normalized bitscore of the best alignment to coding sequences from *E. faecalis* V583.

Figure S1: Example illustrations for assessing quality of homologous gene clusters produced by fai. A) Gene calling or frame-shift differences between the query gene cluster and coding-sequence predictions in the target genome have resulted in a discrepancy for OG_1 (highlighted) from the query being regarded as two separate coding-sequences in the target genome. **B**) Three candidate gene cluster segments located near scaffold edges which match the query gene cluster and meet the thresholds needed for detection as requested in fai in aggregate.

Figure S2: Conservation in the upstream regions of coding sequences of genes in the leporin BGC. The average entropy of the 100 bp upstream regions is shown for each of the genes from the leporin BGC. Coloring of the bars corresponds to effects on BGC expression (for *lepE* and *lepB*) or metabolite production (using a mutant with overexpression of *lepE*) when genes were knocked out as determined by Cary *et al.* 2015.

Figure S3: Influence of dereplication on evolutionary statistics computed by zol. The relationship in values for analogous ortholog groups which map to query proteins from *E. faecalis* V583 for different evolutionary statistics (**A-I**) when different sets of gene clusters corresponding to different approaches in dereplication are shown. Only ortholog groups which lacked any paralogous proteins are shown and accounted for. A line is shown in each plot corresponding to a 1:1 ratio.

Figure S4: The ortholog group with *epa*X features greater diversity relative to other glycosyl transferase related ortholog groups from the *epa* locus in *E. faecalis*. An approximate maximum-likelihood phylogeny based on gap-filtered protein alignments of ortholog groups with domains featuring “glycosyl” and “transferase” as key words. Ortholog groupings (coloring of phylogeny branches) by zol were largely consistent with phylogenetic clades. Association of clades to genes from *E. faecalis* V583 based on sequence alignment are noted.

References

1. Snyder, L., Henkin, T. M., Peters, J. E. & Champness, W. Molecular Genetics of Bacteria, 4th Edition. Preprint at https://doi.org/10.1128/9781555817169 (2013).
2. Price, M. N., Arkin, A. P. & Alm, E. J. The life-cycle of operons. *PLoS Genet.* **2**, e96 (2006).
3. Ptashne, M. *A genetic switch: Gene control and phage. lambda*. (Palo Alto, CA (US); Blackwell Scientific Publications, 1986).
4. Andreu, V. P. *et al.* gutSMASH predicts specialized primary metabolic pathways from the human gut microbiota. *Nature Biotechnology* Preprint at https://doi.org/10.1038/s41587-023-01675-1 (2023).
5. Fischbach, M. A., Walsh, C. T. & Clardy, J. The evolution of gene collectives: How natural selection drives chemical innovation. *Proc. Natl. Acad. Sci. U. S. A.* **105**, 4601–4608 (2008).
6. Gal-Mor, O. & Finlay, B. B. Pathogenicity islands: a molecular toolbox for bacterial

virulence. *Cell. Microbiol.* **8**, 1707–1719 (2006).

7. Kaper, J. B., Nataro, J. P. & Mobley, H. L. Pathogenic Escherichia coli. *Nat. Rev. Microbiol.* **2**, 123–140 (2004).

8. Bolwell, G. P. & Paul Bolwell, G. Biochemistry & Molecular Biology of Plants. *Phytochemistry* vol. 58 185 Preprint at https://doi.org/10.1016/s0031-9422(01)00095-4 (2001).

9. Lindahl, L. & Zengel, J. M. Operon-specific regulation of ribosomal protein synthesis in Escherichia coli. *Proc. Natl. Acad. Sci. U. S. A.* **76**, 6542–6546 (1979).

10. Cordero, O. X. & Polz, M. F. Explaining microbial genomic diversity in light of evolutionary ecology. *Nat. Rev. Microbiol.* **12**, 263–273 (2014).

11. Salamzade, R. *et al.* lsaBGC provides a comprehensive framework for evolutionary analysis of biosynthetic gene clusters within focal taxa. *bioRxiv* 2022.04.20.488953 (2022) doi:10.1101/2022.04.20.488953.

12. Drott, M. T. *et al.* Microevolution in the pansecondary metabolome of Aspergillus flavus and its potential macroevolutionary implications for filamentous fungi. *Proc. Natl. Acad. Sci. U. S. A.* **118**, (2021).

13. Tatusov, R. L., Galperin, M. Y., Natale, D. A. & Koonin, E. V. The COG database: a tool for genome-scale analysis of protein functions and evolution. *Nucleic Acids Res.* **28**, 33–36 (2000).

14. Remm, M., Storm, C. E. & Sonnhammer, E. L. Automatic clustering of orthologs and in-paralogs from pairwise species comparisons. *J. Mol. Biol.* **314**, 1041–1052 (2001).

15. Li, L., Stoeckert, C. J., Jr & Roos, D. S. OrthoMCL: identification of ortholog groups for eukaryotic genomes. *Genome Res.* **13**, 2178–2189 (2003).

16. Edwards, D. J. & Holt, K. E. Beginner's guide to comparative bacterial genome analysis using next-generation sequence data. *Microb. Inform. Exp.* **3**, 2 (2013).

17. Page, A. J. *et al.* Roary: rapid large-scale prokaryote pan genome analysis. *Bioinformatics*

31, 3691–3693 (2015).

18. Emms, D. M. & Kelly, S. OrthoFinder: phylogenetic orthology inference for comparative genomics. *Genome Biol.* **20**, 238 (2019).
19. Medema, M. H., Takano, E. & Breitling, R. Detecting sequence homology at the gene cluster level with MultiGeneBlast. *Mol. Biol. Evol.* **30**, 1218–1223 (2013).
20. Abby, S. S., Néron, B., Ménager, H., Touchon, M. & Rocha, E. P. C. MacSyFinder: a program to mine genomes for molecular systems with an application to CRISPR-Cas systems. *PLoS One* **9**, e110726 (2014).
21. Gilchrist, C. L. M. *et al.* Cblaster: A remote search tool for rapid identification and visualization of homologous gene clusters. *Bioinformatics Advances* **1**, (2021).
22. Navarro-Muñoz, J. C. *et al.* A computational framework to explore large-scale biosynthetic diversity. *Nat. Chem. Biol.* **16**, 60–68 (2020).
23. Georgescu, C. H. *et al.* SynerClust: a highly scalable, synteny-aware orthologue clustering tool. *Microb Genom* **4**, (2018).
24. Tonkin-Hill, G. *et al.* Producing polished prokaryotic pangenomes with the Panaroo pipeline. *Genome Biol.* **21**, 180 (2020).
25. Cosentino, S. & Iwasaki, W. SonicParanoid: fast, accurate and easy orthology inference. *Bioinformatics* **35**, 149–151 (2019).
26. Hu, X. & Friedberg, I. SwiftOrtho: A fast, memory-efficient, multiple genome orthology classifier. *Gigascience* **8**, (2019).
27. Vallenet, D. *et al.* MaGe: a microbial genome annotation system supported by synteny results. *Nucleic Acids Res.* **34**, 53–65 (2006).
28. Stam, M. *et al.* NetSyn: genomic context exploration of protein families. *bioRxiv* (2023) doi:10.1101/2023.02.15.528638.
29. Salamzade, R. *et al.* Evolutionary investigations of the biosynthetic diversity in the skin microbiome using lsaBGC. *Microb Genom* **9**, (2023).

30. Liu, M. *et al.* ICEberg 2.0: an updated database of bacterial integrative and conjugative elements. *Nucleic Acids Res.* **47**, D660–D665 (2019).
31. Terlouw, B. R. *et al.* MIBiG 3.0: a community-driven effort to annotate experimentally validated biosynthetic gene clusters. *Nucleic Acids Res.* **51**, D603–D610 (2023).
32. Bertelli, C. *et al.* IslandViewer 4: expanded prediction of genomic islands for larger-scale datasets. *Nucleic Acids Res.* **45**, W30–W35 (2017).
33. Larralde, M. Pyrodigal: Python bindings and interface to Prodigal, an efficient method for gene prediction in prokaryotes. *J. Open Source Softw.* **7**, 4296 (2022).
34. Hyatt, D. *et al.* Prodigal: prokaryotic gene recognition and translation initiation site identification. *BMC Bioinformatics* **11**, 119 (2010).
35. Li, H. Protein-to-genome alignment with miniprot. *Bioinformatics* **39**, (2023).
36. Grazziotin, A. L., Koonin, E. V. & Kristensen, D. M. Prokaryotic Virus Orthologous Groups (pVOGs): a resource for comparative genomics and protein family annotation. *Nucleic Acids Res.* **45**, D491–D498 (2017).
37. Liu, B., Zheng, D., Jin, Q., Chen, L. & Yang, J. VFDB 2019: a comparative pathogenomic platform with an interactive web interface. *Nucleic Acids Res.* **47**, D687–D692 (2019).
38. Siguier, P., Perochon, J., Lestrade, L., Mahillon, J. & Chandler, M. ISfinder: the reference centre for bacterial insertion sequences. *Nucleic Acids Res.* **34**, D32-6 (2006).
39. Alcock, B. P. *et al.* CARD 2023: expanded curation, support for machine learning, and resistome prediction at the Comprehensive Antibiotic Resistance Database. *Nucleic Acids Res.* **51**, D690–D699 (2023).
40. Kosakovsky Pond, S. L. *et al.* HyPhy 2.5—A Customizable Platform for Evolutionary Hypothesis Testing Using Phylogenies. *Mol. Biol. Evol.* **37**, 295–299 (2019).
41. Thorpe, H. A., Bayliss, S. C., Sheppard, S. K. & Feil, E. J. Piggy: a rapid, large-scale pan-genome analysis tool for intergenic regions in bacteria. *Gigascience* **7**, 1–11 (2018).
42. Gilchrist, C. L. M. & Chooi, Y.-H. clinker & clustermap.js: automatic generation of gene

cluster comparison figures. *Bioinformatics* **37**, 2473–2475 (2021).

43. Hackl, T., Duponchel, S., Barenhoff, K., Weinmann, A. & Fischer, M. G. Virophages and retrotransposons colonize the genomes of a heterotrophic flagellate. *Elife* **10**, (2021).
44. Sullivan, M. J., Petty, N. K. & Beatson, S. A. Easyfig: a genome comparison visualizer. *Bioinformatics* **27**, 1009–1010 (2011).
45. Shaw, J. & Yu, Y. W. Fast and robust metagenomic sequence comparison through sparse chaining with skani. *bioRxiv* 2023.01.18.524587 (2023) doi:10.1101/2023.01.18.524587.
46. Blackwell, G. *et al.* Exploring bacterial diversity via a curated and searchable snapshot of archived DNA. *Access Microbiol.* **4**, (2022).
47. Lebreton, F. *et al.* Emergence of epidemic multidrug-resistant Enterococcus faecium from animal and commensal strains. *MBio* **4**, (2013).
48. Lieberman, T. D. *et al.* Genetic variation of a bacterial pathogen within individuals with cystic fibrosis provides a record of selective pressures. *Nat. Genet.* **46**, 82–87 (2014).
49. Crits-Christoph, A., Olm, M. R., Diamond, S., Bouma-Gregson, K. & Banfield, J. F. Soil bacterial populations are shaped by recombination and gene-specific selection across a grassland meadow. *ISME J.* **14**, 1834–1846 (2020).
50. Hudson, R. R., Slatkin, M. & Maddison, W. P. Estimation of levels of gene flow from DNA sequence data. *Genetics* **132**, 583–589 (1992).
51. Tran, P. Q. & Anantharaman, K. Biogeochemistry Goes Viral: towards a Multifaceted Approach To Study Viruses and Biogeochemical Cycling. *mSystems* **6**, e0113821 (2021).
52. Barr, J. J. *et al.* Bacteriophage adhering to mucus provide a non-host-derived immunity. *Proc. Natl. Acad. Sci. U. S. A.* **110**, 10771–10776 (2013).
53. Lefeuvre, P. *et al.* Evolution and ecology of plant viruses. *Nat. Rev. Microbiol.* **17**, 632–644 (2019).
54. Tran, P. Q. *et al.* Viral impacts on microbial activity and biogeochemical cycling in a seasonally anoxic freshwater lake. *bioRxiv* 2023.04.19.537559 (2023)

768 doi:10.1101/2023.04.19.537559.

769 55. Kieft, K., Zhou, Z. & Anantharaman, K. VIBRANT: automated recovery, annotation and
770 curation of microbial viruses, and evaluation of viral community function from genomic
771 sequences. *Microbiome* **8**, 90 (2020).

772 56. Bok, J. W. *et al.* Genomic mining for Aspergillus natural products. *Chem. Biol.* **13**, 31–37
773 (2006).

774 57. Vadlapudi, V. *et al.* Aspergillus Secondary Metabolite Database, a resource to understand
775 the Secondary metabolome of Aspergillus genus. *Sci. Rep.* **7**, 7325 (2017).

776 58. Robey, M. T., Caesar, L. K., Drott, M. T., Keller, N. P. & Kelleher, N. L. An interpreted atlas
777 of biosynthetic gene clusters from 1,000 fungal genomes. *Proc. Natl. Acad. Sci. U. S. A.*
778 **118**, (2021).

779 59. Hatmaker, E. A. *et al.* Genomic and Phenotypic Trait Variation of the Opportunistic Human
780 Pathogen Aspergillus flavus and Its Close Relatives. *Microbiol Spectr* **10**, e0306922 (2022).

781 60. Xie, H. *et al.* Global multi-omics profiling reveals evolutionary drivers of phylogeographic
782 diversity of fungal specialized metabolism. (2023) doi:10.21203/rs.3.rs-2471999/v1.

783 61. Cary, J. W. *et al.* An Aspergillus flavus secondary metabolic gene cluster containing a
784 hybrid PKS-NRPS is necessary for synthesis of the 2-pyridones, leporins. *Fungal Genet.*
785 *Biol.* **81**, 88–97 (2015).

786 62. Drăgan, M.-A., Moghul, I., Priyam, A., Bustos, C. & Wurm, Y. GeneValidator: identify
787 problems with protein-coding gene predictions. *Bioinformatics* **32**, 1559–1561 (2016).

788 63. Scalzitti, N., Jeannin-Girardon, A., Collet, P., Poch, O. & Thompson, J. D. A benchmark
789 study of ab initio gene prediction methods in diverse eukaryotic organisms. *BMC Genomics*
790 **21**, 293 (2020).

791 64. Skerker, J. M. *et al.* Chromosome assembled and annotated genome sequence of
792 Aspergillus flavus NRRL 3357. *G3* **11**, jkab213 (2021).

793 65. Yang, K., Tian, J. & Keller, N. P. Post-translational modifications drive secondary

metabolite biosynthesis in Aspergillus: a review. *Environ. Microbiol.* **24**, 2857–2881 (2022).

66. Klich, M. A. Aspergillus flavus: the major producer of aflatoxin. *Mol. Plant Pathol.* **8**, 713–722 (2007).

67. Cary, J. W., Ehrlich, K. C., Bland, J. M. & Montalbano, B. G. The Aflatoxin Biosynthesis Cluster Gene, *aflX* , Encodes an Oxidoreductase Involved in Conversion of Versicolorin A to Demethylsterigmatocystin. *Applied and Environmental Microbiology* vol. 72 1096–1101 Preprint at https://doi.org/10.1128/aem.72.2.1096-1101.2006 (2006).

68. Cleveland, T. E. *et al.* Potential of Aspergillus flavus genomics for applications in biotechnology. *Trends Biotechnol.* **27**, 151–157 (2009).

69. Ehrlich, K. C., Li, P., Scharfenstein, L. & Chang, P.-K. HypC, the anthrone oxidase involved in aflatoxin biosynthesis. *Appl. Environ. Microbiol.* **76**, 3374–3377 (2010).

70. Xu, Y., Murray, B. E. & Weinstock, G. M. A cluster of genes involved in polysaccharide biosynthesis from Enterococcus faecalis OG1RF. *Infect. Immun.* **66**, 4313–4323 (1998).

71. Palmer, K. L. *et al.* Comparative Genomics of Enterococci: Variation in Enterococcus faecalis, Clade Structure in E. faecium, and Defining Characteristics of *E . gallinarum* and *E . casseliflavus*. *mBio* vol. 3 Preprint at https://doi.org/10.1128/mbio.00318-11 (2012).

72. Hancock, L. E., Murray, B. E. & Sillanpää, J. Enterococcal Cell Wall Components and Structures. in *Enterococci: From Commensals to Leading Causes of Drug Resistant Infection* (eds. Gilmore, M. S., Clewell, D. B., Ike, Y. & Shankar, N.) (Massachusetts Eye and Ear Infirmary, 2014).

73. Qin, X. *et al.* Complete genome sequence of Enterococcus faecium strain TX16 and comparative genomic analysis of Enterococcus faecium genomes. *BMC Microbiol.* **12**, 135 (2012).

74. Teng, F., Jacques-Palaz, K. D., Weinstock, G. M. & Murray, B. E. Evidence that the Enterococcal Polysaccharide Antigen Gene (*epa*) Cluster Is Widespread in *Enterococcus faecalis* and Influences Resistance to Phagocytic Killing of *E. faecalis*. *Infection and*

Immunity vol. 70 2010–2015 Preprint at https://doi.org/10.1128/iai.70.4.2010-2015.2002 (2002).

75. Teng, F., Singh, K. V., Bourgogne, A., Zeng, J. & Murray, B. E. Further Characterization of the *epa* Gene Cluster and Epa Polysaccharides of *Enterococcus faecalis*. *Infection and Immunity* vol. 77 3759–3767 Preprint at https://doi.org/10.1128/iai.00149-09 (2009).
76. Rigottier-Gois, L. *et al.* The surface rhamnopolysaccharide epa of Enterococcus faecalis is a key determinant of intestinal colonization. *J. Infect. Dis.* **211**, 62–71 (2015).
77. Guerardel, Y. *et al.* Complete structure of the enterococcal polysaccharide antigen (EPA) of vancomycin-resistant Enterococcus faecalis V583 reveals that EPA decorations are teichoic acids covalently linked to a rhamnopolysaccharide backbone. *MBio* **11**, (2020).
78. Smith, R. E. *et al.* Decoration of the enterococcal polysaccharide antigen EPA is essential for virulence, cell surface charge and interaction with effectors of the innate immune system. *PLoS Pathog.* **15**, e1007730 (2019).
79. Singh, K. V. & Murray, B. E. Loss of a Major Enterococcal Polysaccharide Antigen (Epa) by Enterococcus faecalis Is Associated with Increased Resistance to Ceftriaxone and Carbapenems. *Antimicrob. Agents Chemother.* **63**, (2019).
80. Ho, K., Huo, W., Pas, S., Dao, R. & Palmer, K. L. Loss-of-Function Mutations in *epaR* Confer Resistance to □NPV1 Infection in Enterococcus faecalis OG1RF. *Antimicrobial Agents and Chemotherapy* vol. 62 Preprint at https://doi.org/10.1128/aac.00758-18 (2018).
81. Fiore, E., Van Tyne, D. & Gilmore, M. S. Pathogenicity of Enterococci. *Microbiol Spectr* **7**, (2019).
82. Lebreton, F., Willems, R. J. L. & Gilmore, M. S. Enterococcus Diversity, Origins in Nature, and Gut Colonization. in *Enterococci: From Commensals to Leading Causes of Drug Resistant Infection* (eds. Gilmore, M. S., Clewell, D. B., Ike, Y. & Shankar, N.) (Massachusetts Eye and Ear Infirmary, 2014).
83. Lebreton, F. *et al.* Tracing the Enterococci from Paleozoic Origins to the Hospital. *Cell* **169**,

849-861.e13 (2017).

84. Schwartzman, J. A. *et al.* Global diversity of enterococci and description of 18 novel species. *bioRxiv* 2023.05.18.540996 (2023) doi:10.1101/2023.05.18.540996.

85. Parks, D. H. *et al.* GTDB: an ongoing census of bacterial and archaeal diversity through a phylogenetically consistent, rank normalized and complete genome-based taxonomy. *Nucleic Acids Res.* (2021) doi:10.1093/nar/gkab776.

86. Reid, K. C., Cockerill, F. R., III & Patel, R. Clinical and epidemiological features of Enterococcus casseliflavus/flavescens and Enterococcus gallinarum bacteremia: a report of 20 cases. *Clin. Infect. Dis.* **32**, 1540–1546 (2001).

87. Monticelli, J., Knezevich, A., Luzzati, R. & Di Bella, S. Clinical management of non-faecium non-faecalis vancomycin-resistant enterococci infection. Focus on Enterococcus gallinarum and Enterococcus casseliflavus/flavescens. *J. Infect. Chemother.* **24**, 237–246 (2018).

88. Nevers, Y. *et al.* The Quest for Orthologs orthology benchmark service in 2022. *Nucleic Acids Res.* (2022).

89. Dale, J. L., Cagnazzo, J., Phan, C. Q., Barnes, A. M. T. & Dunny, G. M. Multiple Roles for Enterococcus faecalis Glycosyltransferases in Biofilm-Associated Antibiotic Resistance, Cell Envelope Integrity, and Conjugative Transfer. *Antimicrobial Agents and Chemotherapy* vol. 59 4094–4105 Preprint at https://doi.org/10.1128/aac.00344-15 (2015).

90. Olm, M. R., Brown, C. T., Brooks, B. & Banfield, J. F. dRep: a tool for fast and accurate genomic comparisons that enables improved genome recovery from metagenomes through de-replication. *ISME J.* **11**, 2864–2868 (2017).

91. Jain, C., Rodriguez-R, L. M., Phillippy, A. M., Konstantinidis, K. T. & Aluru, S. High throughput ANI analysis of 90K prokaryotic genomes reveals clear species boundaries. *Nat. Commun.* **9**, 1–8 (2018).

92. van den Belt, M. *et al.* CAGECAT: The CompArative GEne Cluster Analysis Toolbox for rapid search and visualisation of homologous gene clusters. *BMC Bioinformatics* **24**, 181

(2023).

93. Bertelli, C. *et al.* Enabling genomic island prediction and comparison in multiple genomes to investigate bacterial evolution and outbreaks. *Microb. Genom.* **8**, (2022).

94. Zablocki, O., Jang, H. B., Bolduc, B. & Sullivan, M. B. VConTACT 2: A tool to automate genome-based prokaryotic viral taxonomy. in *Plant and Animal Genome XXVII Conference
(January 12- 16, 2019)* (PAG, 2019).

95. Salamzade, R. *et al.* Inter-species geographic signatures for tracing horizontal gene transfer and long-term persistence of carbapenem resistance. *Genome Med.* **14**, 37 (2022).

96. Sheppard, A. E. *et al.* Nested Russian Doll-Like Genetic Mobility Drives Rapid Dissemination of the Carbapenem Resistance Gene blaKPC. *Antimicrob. Agents Chemother.* **60**, 3767–3778 (2016).

97. Groussin, M. *et al.* Elevated rates of horizontal gene transfer in the industrialized human microbiome. *Cell* **184**, 2053-2067.e18 (2021).

98. Crits-Christoph, A., Diamond, S., Butterfield, C. N., Thomas, B. C. & Banfield, J. F. Novel soil bacteria possess diverse genes for secondary metabolite biosynthesis. *Nature* **558**, 440–444 (2018).

99. Bickhart, D. M. *et al.* Generation of lineage-resolved complete metagenome-assembled genomes by precision phasing. *bioRxiv* 2021.05.04.442591 (2021) doi:10.1101/2021.05.04.442591.

100. Chatterjee, A. *et al.* Bacteriophage Resistance Alters Antibiotic-Mediated Intestinal Expansion of Enterococci. *Infect. Immun.* **87**, (2019).

101. Chatterjee, A. *et al.* Parallel genomics uncover novel enterococcal-bacteriophage interactions. Preprint at https://doi.org/10.1101/858506.

102. Canfield, G. S. *et al.* Lytic bacteriophages facilitate antibiotic sensitization of *Enterococcus faecium*. Preprint at https://doi.org/10.1101/2020.09.22.309401.

103. van Tilburg Bernardes, E., Charron-Mazenod, L., Reading, D. J., Reckseidler-Zenteno, S.

L. & Lewenza, S. Exopolysaccharide-repressing small molecules with antibiofilm and antivirulence activity against Pseudomonas aeruginosa. *Antimicrob. Agents Chemother.* **61**, (2017).

104. Shen, Y. & Loessner, M. J. Beyond antibacterials - exploring bacteriophages as antivirulence agents. *Curr. Opin. Biotechnol.* **68**, 166–173 (2021).

105. Shankar-Sinha, S. *et al.* The Klebsiella pneumoniae O antigen contributes to bacteremia and lethality during murine pneumonia. *Infect. Immun.* **72**, 1423–1430 (2004).

106. Zhao, S. *et al.* Adaptive evolution within gut microbiomes of healthy people. *Cell Host Microbe* **25**, 656-667.e8 (2019).

107. Grüning, B. *et al.* Bioconda: sustainable and comprehensive software distribution for the life sciences. *Nat. Methods* **15**, 475–476 (2018).

108. Cock, P. J. A. *et al.* Biopython: freely available Python tools for computational molecular biology and bioinformatics. *Bioinformatics* **25**, 1422–1423 (2009).

109. Capella-Gutiérrez, S., Silla-Martínez, J. M. & Gabaldón, T. trimAl: a tool for automated alignment trimming in large-scale phylogenetic analyses. *Bioinformatics* **25**, 1972–1973 (2009).

110. Price, M. N., Dehal, P. S. & Arkin, A. P. FastTree 2--approximately maximum-likelihood trees for large alignments. *PLoS One* **5**, e9490 (2010).

111. Huang, Y., Niu, B., Gao, Y., Fu, L. & Li, W. CD-HIT Suite: a web server for clustering and comparing biological sequences. *Bioinformatics* **26**, 680–682 (2010).

112. Eddy, S. R. Accelerated Profile HMM Searches. *PLoS Comput. Biol.* **7**, e1002195 (2011).

113. Buchfink, B., Xie, C. & Huson, D. H. Fast and sensitive protein alignment using DIAMOND. *Nat. Methods* **12**, 59–60 (2014).

114. Schreiber, J. Pomegranate: fast and flexible probabilistic modeling in python. *J. Mach. Learn. Res.* (2017).

115. Edgar, R. C. Muscle5: High-accuracy alignment ensembles enable unbiased assessments

924 of sequence homology and phylogeny. *Nat. Commun.* **13**, 6968 (2022).

925 116. Blin, K. *et al.* antiSMASH 6.0: improving cluster detection and comparison capabilities.

926 *Nucleic Acids Res.* **49**, W29–W35 (2021).

927 117. Ondov, B. D. *et al.* Mash: fast genome and metagenome distance estimation using

928 MinHash. *Genome Biol.* **17**, 132 (2016).

929 118. Paradis, E., Claude, J. & Strimmer, K. APE: Analyses of Phylogenetics and Evolution in R

930 language. *Bioinformatics* **20**, 289–290 (2004).

931 119. Majoros, W. H., Pertea, M. & Salzberg, S. L. TigrScan and GlimmerHMM: two open source

932 ab initio eukaryotic gene-finders. *Bioinformatics* **20**, 2878–2879 (2004).

933 120. Olm, M. R. *et al.* Consistent Metagenome-Derived Metrics Verify and Delineate Bacterial

934 Species Boundaries. *mSystems* **5**, (2020).

935 121. Mistry, J. *et al.* Pfam: The protein families database in 2021. *Nucleic Acids Res.* **49**, D412–

936 D419 (2021).

937 122. Letunic, I. & Bork, P. Interactive Tree Of Life (iTOL) v4: recent updates and new

938 developments. *Nucleic Acids Res.* **47**, W256–W259 (2019).

939

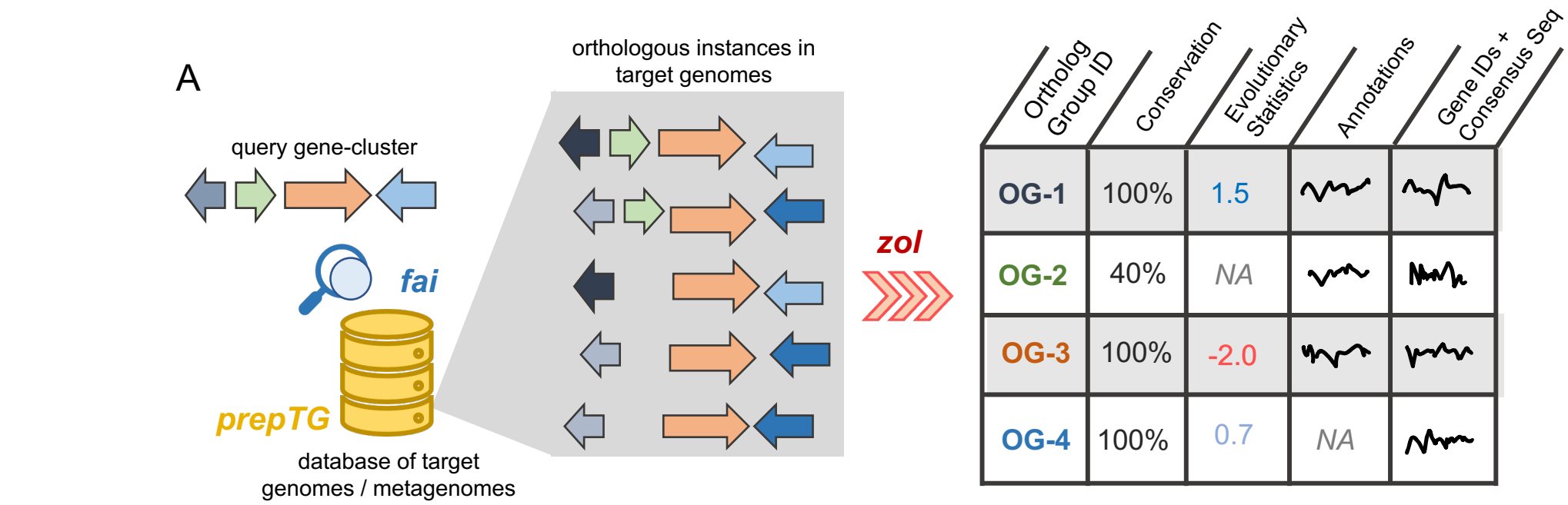

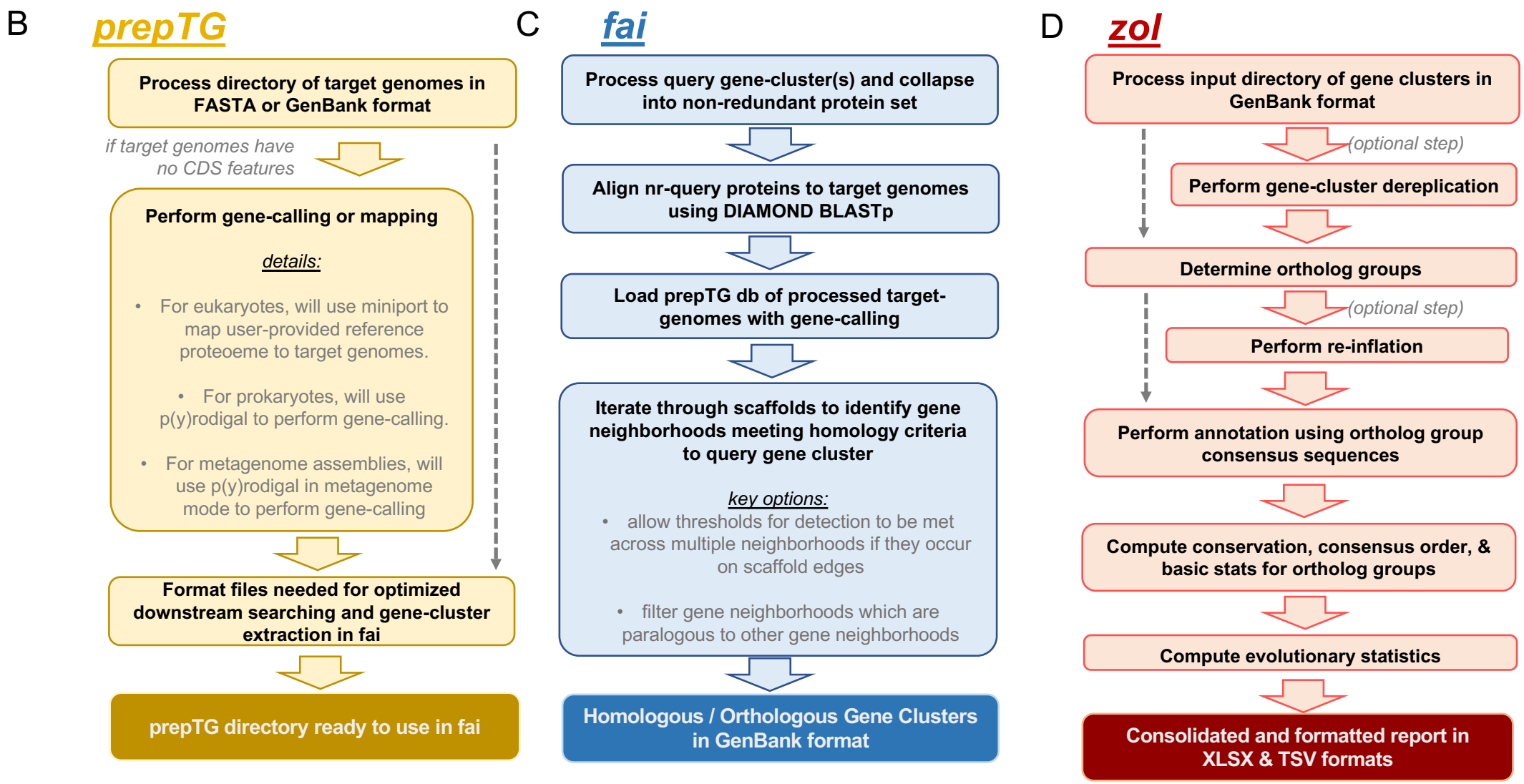

Figure 1: Overviews of fai and zol. A) A schematic of how prepTG, fai, and zol are integrated to perform evolutionary investigations by searching for gene-clusters. An overview of the prepTG (**B**), fai (**C**) and zol (**D**) algorithms and workflows.

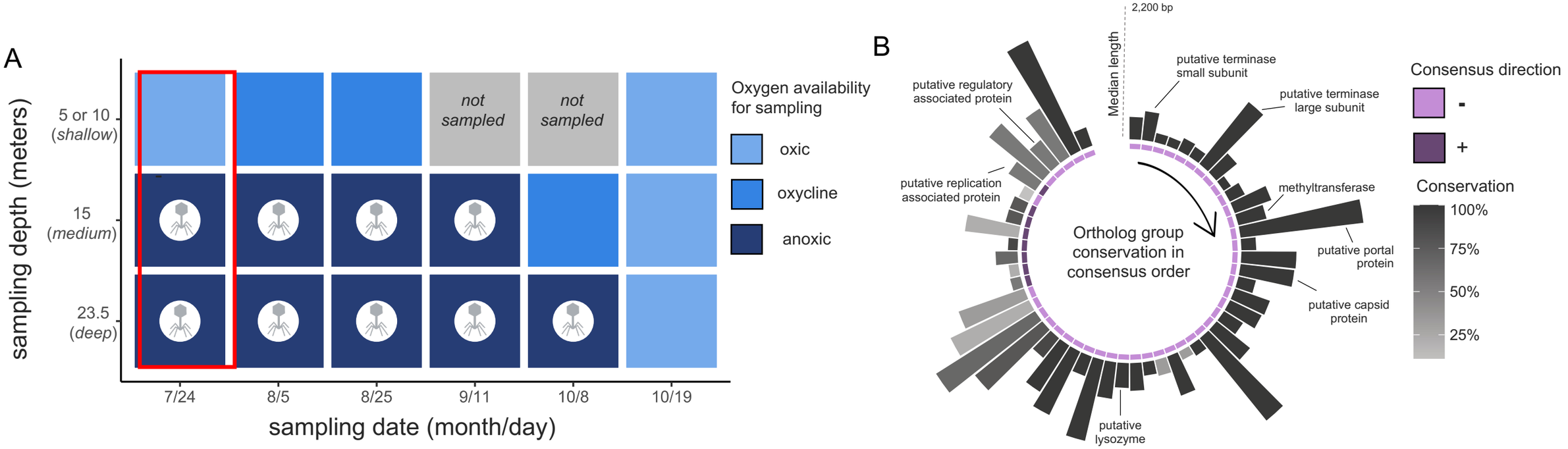

Figure 2: Targeted viral detection in metagenomes using fai. A) Total metagenomes from a single site in Lake Mendota across multiple depths and timepoints from Tran et al. 2023 were investigated using fai for the presence of a virus found in two of the three earliest microbiome samplings (red box). The presence of the virus is indicated by a phage icon. Metagenome samples are colored according to whether they corresponded to oxic, oxycline, or anoxic. The most shallow sampling depths varied for different dates and consolidated as a single row corresponding to a sampling depth of either 5 or 10 meters. **B**) The pangenome of the virus is shown based on the consensus order and directionality of coding sequences inferred by zol. Bar heights correspond to the median length of coding sequences and are colored based on the percentages of the nine metagenomes the virus was detected in. BioRender was used in generation of this figure.

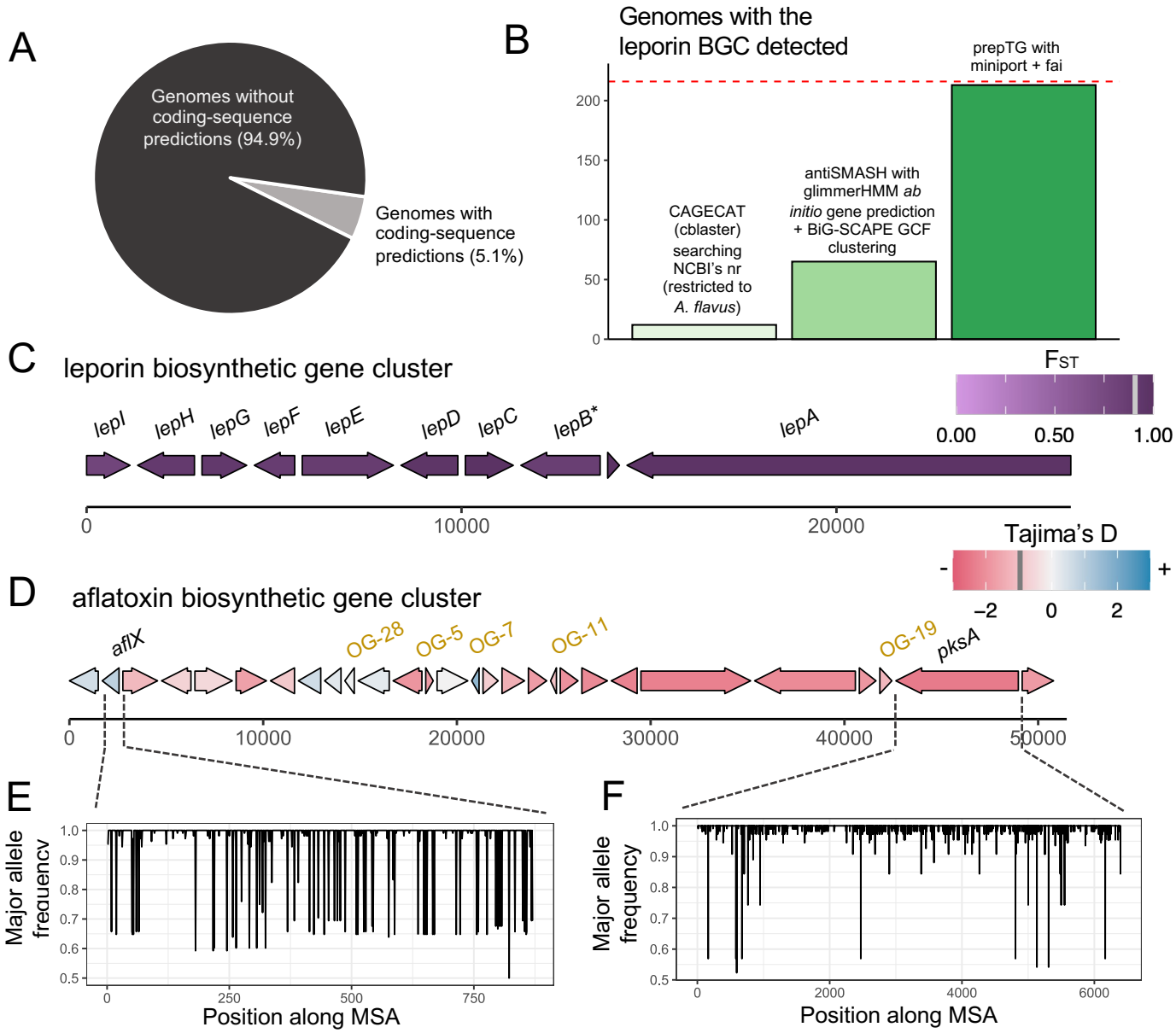

Figure 3: Evolutionary trends of common BGCs in *A. flavus*. A) The proportion of 216 A. flavus genomes from NCBI's GenBank database with coding-sequence predictions available. **B)** Comparison of the sensitivity of fai and alternate approaches based on assemblies for detecting the leporin BGC. The red-line indicates the total number of genomes (n=216) assessed. A schematic of the (**C**) leporin and (**D**) aflatoxin BGCs is shown with genes present in ≥ 10% of samples shown in consensus order and relative directionality. Coloring of genes in (**C**) corresponds to FST values and in (**D**) to Tajima's D values, as calculated by zol. Grey bars in the legends, at (C) 0.92 and (D) -0.98, indicate the mean values for the statistics across genes in the BGC. *For the leporin BGC, *lepB* corresponds to an updated open-reading frame (ORF) prediction by Skerker *et al.* 2021 which was the combination of AFLA_066860 and AFLA_066870 ORFs in the MIBiG entry BGC0001445 used as the query for fai. For the aflatoxin BGC, ORFs which were not represented in the MIBiG entry BGC0000008 but predicted to be within the aflatoxin BGC by mapping of gene-calls from *A. flavus* NRRL 3357 by Skerker et al. 2021 are shown in gold. The major allele frequency distributions are shown for (**E**) *aflX* and (**F**) *pksA*, which depict opposite trends in sequence conservation according to their respective Tajima's D calculations.

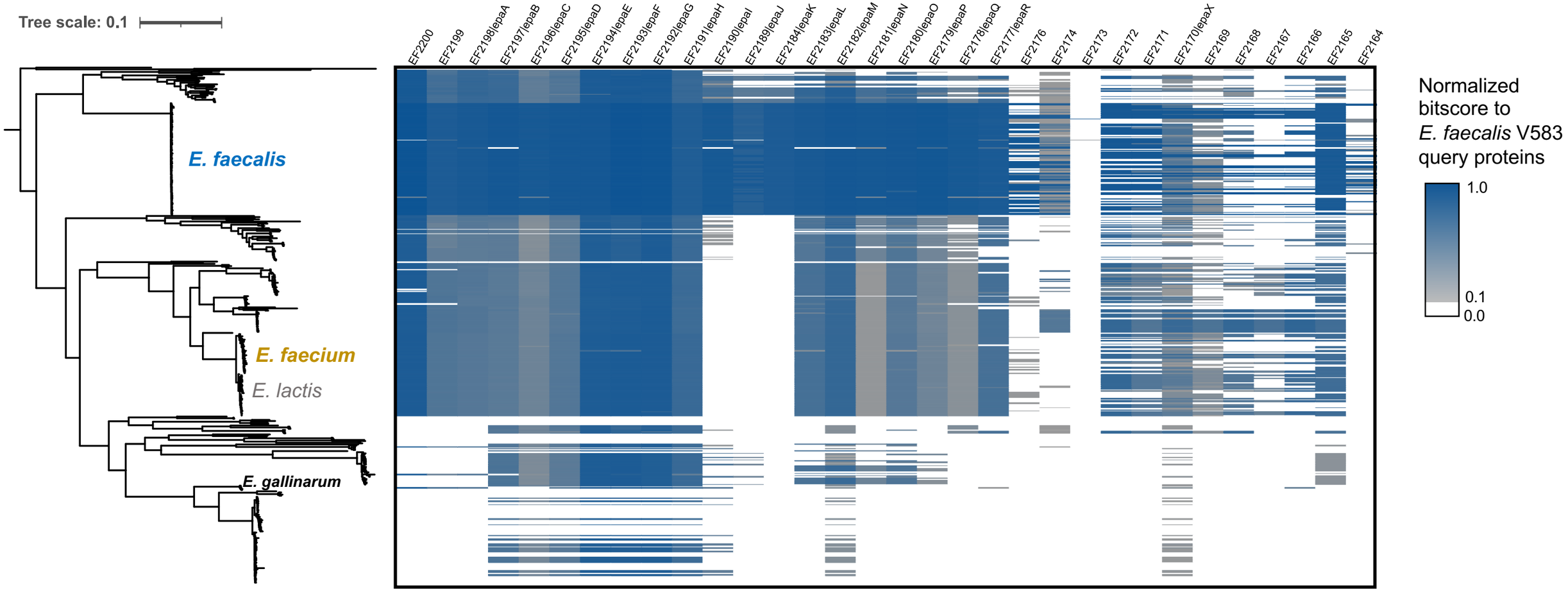

Figure 4: The *epa* locus is conserved across most enterococcal species. The distribution of the *epa* locus and associated genes, based on criteria used for running fai, is shown across 463 representative genomes across *Enterococcus*. Coloring of the heatmap corresponds to the normalized bitscore of the best alignment to coding sequences from *E. faecalis* V583.

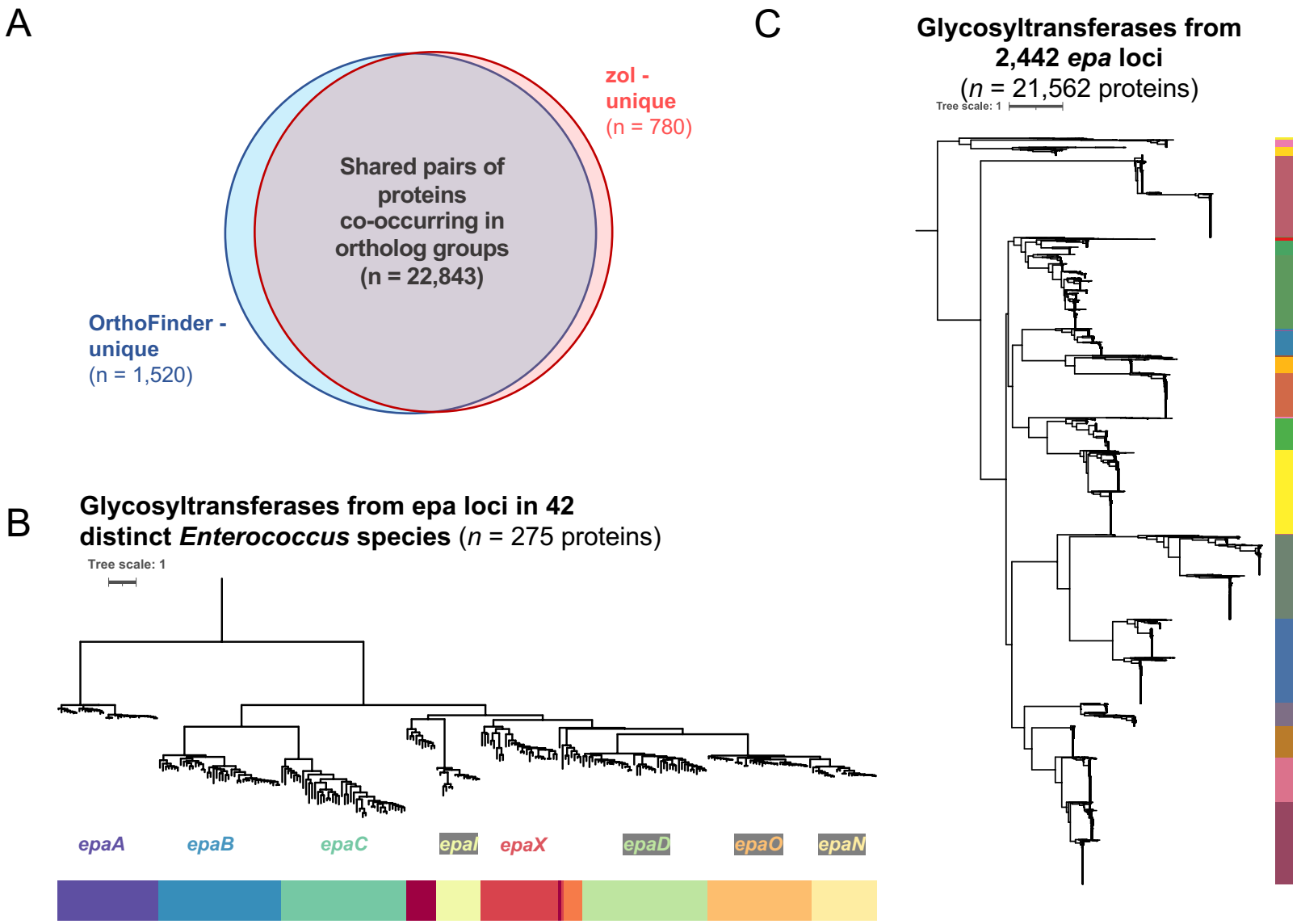

Figure 5: Assessment of gene-cluster restricted ortholog grouping by fai and zol. A) zol gene-cluster constricted ortholog group predictions for *epa* locus proteins from 42 distinct representative enterococcal species were compared to genome-wide predictions of ortholog groups by OrthoFinder. A phylogeny based on gap-filtered protein alignments of ortholog groups with domains featuring “glycosyl” and “transferase” as key words is shown from (**B**) *epa* loci in the 42 representative genomes and (**C**) a more comprehensive set of 2,442 *epa* loci. Each node represents a specific protein and coloring of the track corresponds to their ortholog group designations by zol. Note, (B) 2 (0.07%) and (C) 79 proteins (0.4%) were removed prior to phylogeny construction due to an abundance of gaps in the trimmed alignment.

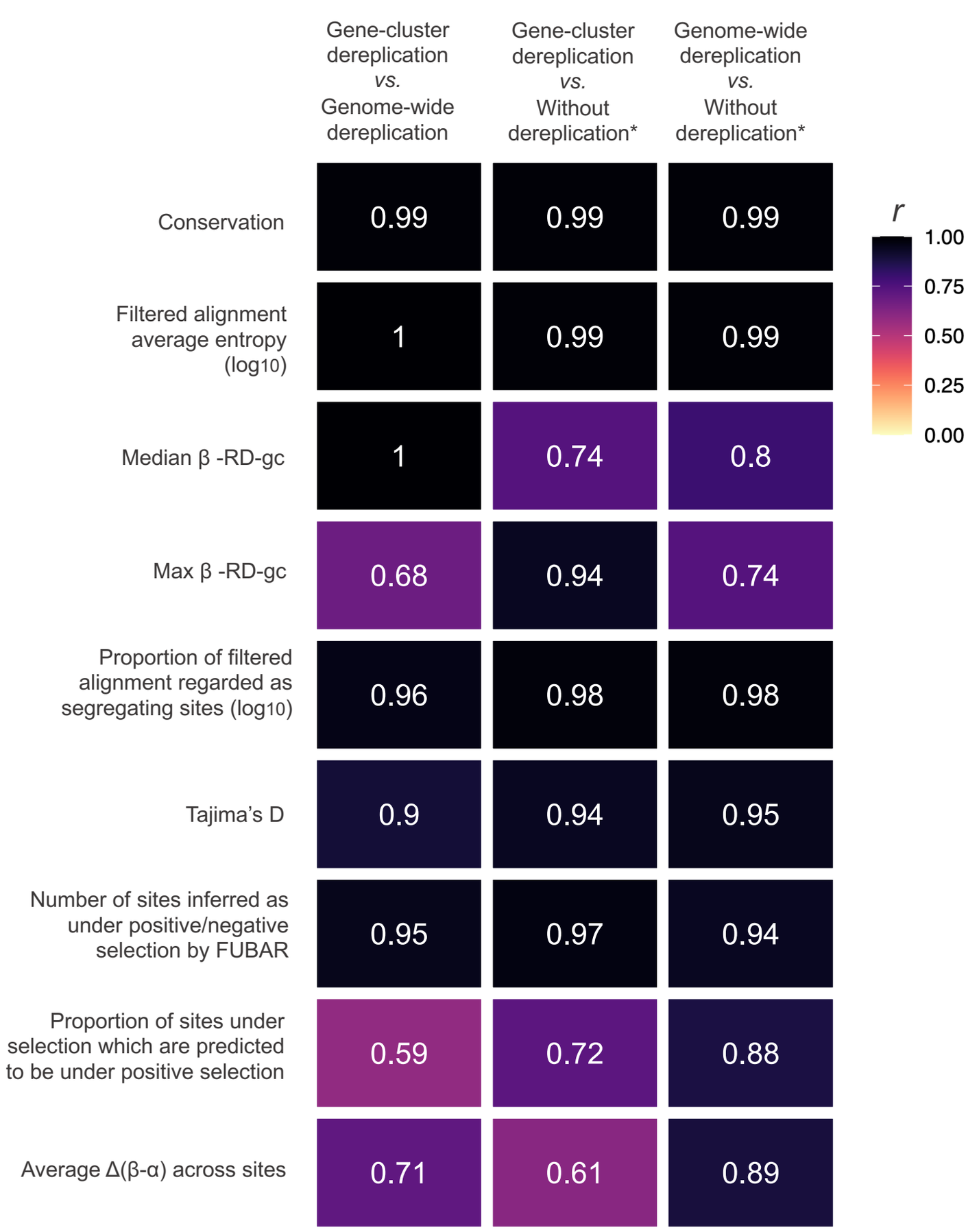

Figure 6: Effects of dereplication on the calculation of evolutionary statistics by zol. The heatmap shows the correlation of values for analogous ortholog groups for various evolutionary statistics computed by zol when different approaches to dereplication are used. See Methods for further details. *To simulate no dereplication, gene-cluster dereplication with re-inflation parameters were used in zol.

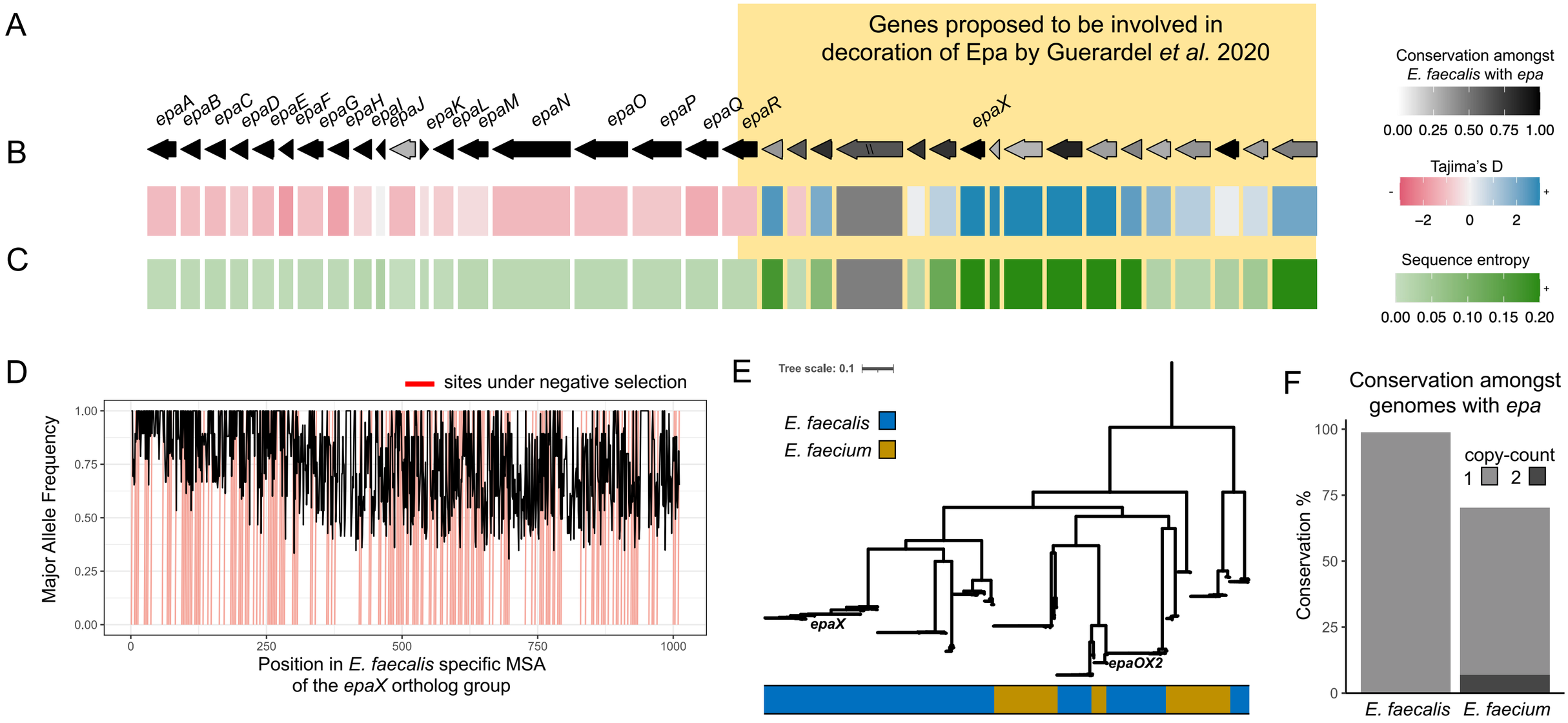

Figure 7: Distribution of the *epa* locus and associated genes across the genus of *Enterococcus*. A) A schematic is shown for the *epa* locus in *E. faecalis* for genes which were found in ≥ 25% of 83 representative genomes for the species presented in consensus order with consensus directionality as inferred by zol. The coloring corresponds to the conservation of individual genes. Genes upstream and/or including *epaR* were recently proposed to be involved in decoration of Epa by Guerardel *et al.* 2020. "//" indicates that the ortholog group was not single-copy in the context of the gene-cluster. The tracks below the gene showcase their sequence similarity across the *E. faecalis* genomes measured using (**B**) Tajima's D and (**C**) the average sequence alignment entropy. **D**) The major allele frequency is depicted across the alignment for the ortholog group featuring *epaX*. Sites predicted to be under negative selection by FUBAR, Prob(α>β) ≥ 0.9, are marked in red. **E**) An approximate maximum-likelihood phylogeny based on gap-filtered codon alignments for the ortholog group corresponding to *epaX* and *epaX*-like proteins in the joint *E. faecalis* and *E. faecium* investigation of the epa locus using zol. **F**) Conservation of *epaX* is shown amongst *E. faecalis* and *E. faecium* genomes with a high-quality representation of the *epa* locus available. Coloring of the bars corresponds to the proportion of genomes with a certain copy-count of the *epaX*-like ortholog group.